SMAR 2017 – Fourth Conference on Smart Monitoring,
Assessment and Rehabilitation of Civil Structures

SMAR 2017

Functional properties of Fe-based shape memory alloys containing finely dispersed precipitates

P. Krooß[1], M. Vollmer[1], C. Somsen[2], Y.I. Chumlyakov[3], T. Niendorf[1]

[1] Institut für Werkstofftechnik, Universität Kassel, 34125 Kassel, Germany
[2] Institut für Werkstoffkunde, Ruhr-Universität Bochum, 44780 Bochum, Germany
[3] Siberian Physical Technical Institute, Tomsk State University, 634050 Tomsk, Russia

Shape memory alloys (SMAs) attract a lot of attention due to their unique properties, making them excellent candidates for actuation and damping applications in numerous industry sectors. However, well established SMAs such as Ni-Ti are limited to niche applications as they suffer from high processing costs. Since well-established processing routes from steel industry are suited for fabrication of Fe-based SMAs (Fe-SMAs), these alloy systems are promising candidates for overcoming the current roadblocks. Besides a deep knowledge of adapted processing parameters, cyclic instability is a key issue preventing widespread applications so far. The current study highlights the pseudoelastic cyclic behavior of two different Fe-SMAs. Functional fatigue tests were conducted in order to identify microstructural features accountable for functional degradation. Microstructural analyses revealed that increased dislocation activity leads to significant evolution of irreversible strain during pseudoelastic cycling.

1 INTRODUCTON

Due to their superior properties shape memory alloys (SMAs) attracted a lot of attention in recent decades [1-4]. Binary Ni-Ti SMAs, being the most studied SMA in the last century, show promising functional material properties for damping and actuation applications, i.e. high recoverable transformation strains and high bearable stresses accompanied by good cyclic stability [1-4]. However, conventional Ni-Ti SMAs are limited to niche applications, e.g. in the medical sector, due to costly processing routes needed to obtain suitable functional properties [1-4]. Thus, numerous SMAs have been investigated in order to reduce processing complexity and increase cost efficiency [1-4]. In this regard, two newly developed Fe-based SMAs seem to overcome previous issues. Fe-Ni-Co-Al-X and Fe-Mn-Al-Ni-X are very promising due to the fact that established processing routes from steel industry are well suited for the fabrication of SMA components [1-8]. However, opposite to conventional binary Ni-Ti SMAs, most Fe-based SMAs suffer from rapid functional degradation during cyclic loading. This is mainly attributed to a high dislocation density and/or a high degree of crystallographic anisotropy, which results in pronounced pinning of evolving martensite phase boundaries making phase transformation irreversible [9-11]. However, data reporting on the cyclic degradation mechanisms of Fe-based SMAs are still rare in literature. Thus, this study outlines the main degradation mechanisms in two recently developed Fe-based SMA systems, being very promising candidates for future damping applications, i.e. large damping devices in civil engineering, e.g. to be used in earthquake resistant buildings.

2 MATERIALS AND EXPERIMENTAL DETAILLS

Ingots of $Fe_{41}Ni_{28}Co_{17}Al_{11.5}Ta_{2.5}$ (at. %) SMAs were produced using vacuum induction melting. For growing single crystalline material the Bridgman technique was used in a helium atmosphere. Dog-bone shaped tensile specimens with a cross section of 1.5 mm x 1.5 mm in the gauge length were electro discharge machined out of the single crystals with their crystallographic [001]-orientation parallel to the loading direction. For homogenization of the samples solution annealing was carried out at 1300 °C for 12 h followed by a short time aging treatment at 700 °C for 1 h. Ingots of $Fe_{44.3}$ $Mn_{34.8}$ $Al_{13.5}$ $Ni_{7.4}$ (at. %) were produced by vacuum induction melting. Dog-bone shaped specimens with a cross section of 1.6 mm x 1.5 mm were electro discharge machined from the bulk material. Solution treatment and subsequent cyclic heat treatments between the single phase region (1200 °C) and the ($\alpha + \gamma$) two-phase region (900 °C) were conducted to stimulate abnormal grain growth (AGG) to obtain a bamboo-like structure followed by quenching in tempered water. Ageing was conducted at 200 °C to introduce coherent β-phase precipitates.

For the characterization of the mechanical functional properties, servo-hydraulic testing machines were used. Systems were equipped with extensometers, which were directly attached to the sample surfaces. *In situ* optical and electron microscopy studies were conducted in order to correlate the global phase transformation behavior with local microstructural evolution upon mechanical cycling. For further details on the experimental details and sample preparation the reader is referred to Refs. [9-11].

3 RESULTS AND DISCUSSION

3.1 Functional fatigue – basic considerations

Figure 1 shows a schematic pseudoelastic curve illustrating charactristic values for the evaluation of the cyclic stability of SMAs.

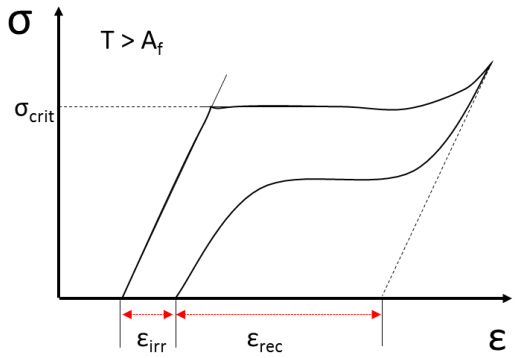

Figure 1: Schematic illustration of a pseudoelastic curve highlighting functional degradation ($T>A_f$).

At σ_{crit} the stress induced austenite to martensite transformation starts. The plateau stress hardly changes until the material is transformed to 100 % martensite, followed by an elastic deformation of the martensitic phase. Upon unloading the reverse transformation from martensite to austenite takes place, again revealing a plateau-like character. Whereas ε_{irr} defines the irrecoverable amount of transformation strain, ε_{rec} represents the amount of transformation strain that has been recovered upon unloading. The absolute values of transformation strain and stress as well as the recovery ratio (relation of the amount of recovered stain and the transformation strain) strongly depend on

the alloy system and, thus, on the crystallography of the phases being present. Furthermore, the general material strength, i.e. the resistance against dislocation glide, is an important factor [1-4].

3.2 Functional properties of $Fe_{41}Ni_{28}Co_{17}Al_{11.5}Ta_{2.5}$ (at. %) SMA

Recent studies revealed that Fe-Ni-Co-Al-Ta SMAs show promising functional properties. However, microstructural processing is complex since only strongly textured polycrystalline conditions allow for good functional properties [8]. Due to the precipitation of the brittle β–phase at the grain boundaries, grain boundary cracking is strongly promoted upon deformation [8,13]. The addition of B reduces precipitation of the brittle β–phase [8,13]. However, due to the pronounced anisotropy, strong textured material is still needed. In this study, single crystalline material is in focus of experiments in order to exclude the impact of grain boundary cracking on general functional fatigue properties.

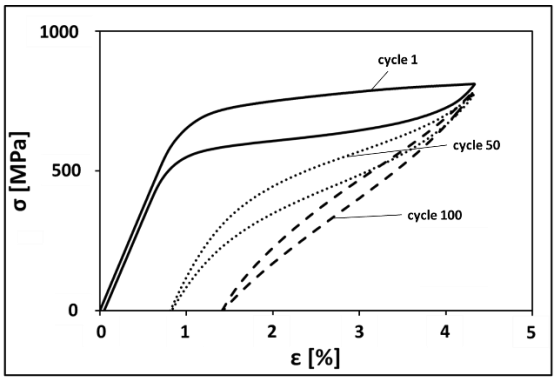

Figure 2: Cyclic stress - strain response of a ⟨001⟩ oriented Fe-Ni-Co-Al-Ta shape memory single crystal at ambient temperature [9].

Figure 2a shows the cyclic stress - strain response of a ⟨001⟩ oriented Fe-Ni-Co-Al-Ta SMA single crystal at ambient temperature. The sample was solutionized at 1300 °C for 12 h and subsequently aged for 1h at 700 °C [9]. Aging in temperature regimes between 600 °C and 700 °C results in the formation of finely dispersed γ´ - precipitates [9].

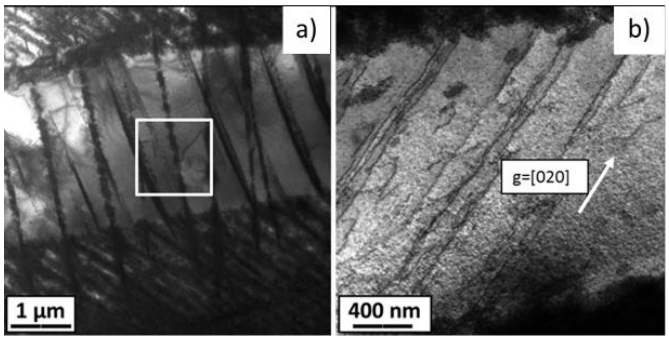

Figure 3: TEM analysis of the prevailing microstructure after fatigue (100 pseudoelastic cycles at RT); a) overview image, b) dislocation structures at higher magnification [9].

Form the cyclic stress-strain response it is obvious that the shape recovery decreases distinctly with increasing cycle number. Whereas in the first cyclic the recoverability is almost 100 %, in cycles 50 and 100 about 0.9 % and 1.5 % irreversible strain, respectively, are accumulated. Thus, the shape recovery ratio decreases. It is well known that an interaction of different martensite variants as well as insufficient matrix hardness can lead to cyclic instability due to the formation

of dislocations, which are able to pin evolving martensite phases [8-9,13]. Figure 3a shows the microstructure after fatigue testing. The dark contrast features in Figure 3a were identified as the stress induced tetragonal martensite phase [9]. Figure 3b shows a TEM image revealing that a high dislocation activity is present in the microstructure [9]. Thus, it can be deduced that a strong interaction of the martensite variants, which has been observed by *in situ* tests [9], led to an increased dislocation activity. The microstructure appears to be composed of a high amount of differently oriented martensite variants, being pinned in the austenite matrix. This pinning mechanisms was also detailed in other studies and corresponding degradation mechanisms were derived [14-18].

Besides the role of the intensive interaction of martensite variants, the additional impact of the finely dispersed γ´- particles was analyzed [9]. Figure 4 shows TEM images of the nano-scaled precipitates in the fatigued FCC – matrix. Figures 4a and b reveal that all three phases, i.e. FCC austenite, BCT martensite and and γ´- precipitates, are simultaneously present in the microstructure. The high-resolution TEM analysis shown in Figure 4d) indicates that the tetragonal BCT martensite phase is present in the vicinity of the γ´- precipitates. Due to the fact that the martensite phase was found in the direct vicinity of the γ´- precipitates two possible mechanism can be derived that may contribute to functional degradation. First, the coherency stress field surrounding the particle can provide for a specific amount of intrinsic mechanical energy to stabilize the martensitic phase in the vicinity of the precipitates. Second, due to the interaction of differently oriented martensite variants the particle undergoes a double-shear deformation, resulting in plasticity and concomitant pinning of phase boundaries [9]. Thus, in Fe-Ni-Co-Al-Ta Fe-based SMAs two degradation mechanisms have be accounted for functional degradation at RT, however, separation is currently hardly feasible.

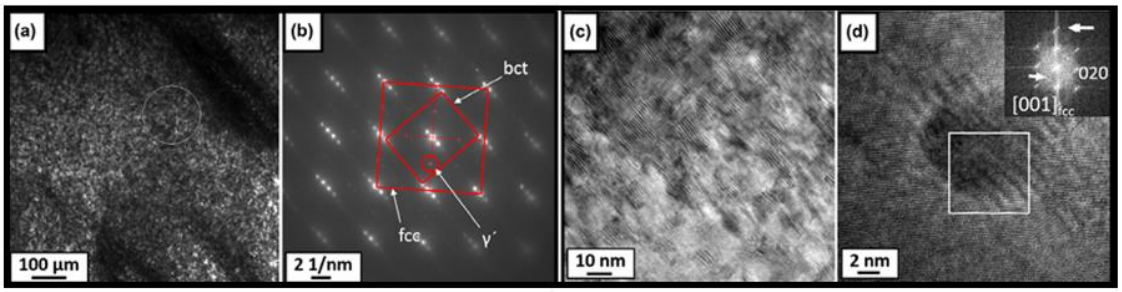

Figure 4: TEM images revealing the presence of γ´- precipitates within the fatigued FCC matrix. In a) the area of interest is shown, b) selected area diffraction (SAD) image of the area in a); the diffraction peaks of BCT martensite, FCC austenite and γ´- precipitates are indexed; c) overview of the precipitates within the FCC matrix and d) high resolution image indicating martensite in the direct vicinity of the particle. (Recompiled from [9]).

3.3 Functional properties of $Fe_{44.3}Mn_{34.8}Al_{13.5}Ni_{7.4}$ (at. %) SMA

Fe-Mn-Al-Ni SMAs show excellent material properties [5,11,19-21]. Theoretical calculations based on the energy minimization theory revealed that up to 26 % percent of transformation strain can be reached in this alloy system [21]. However, to the best of the authors' knowledge not more than 12 % transformation strain in single crystalline state and 6.7 % strain in polycrystalline condition have been observed experimentally up to now [5,11,19-21]. Similar to the Fe-Ni-Co-Al-Ta SMA detailed in the previous chapter, Fe-Mn-Al-Ni SMA also require small, finely dispersed precipitates, which make transformation thermoelastic [5,11,19-21]. Figure 5c shows the β–type precipitates within the α-Matrix. The diameter of the β–precipitates is similar to those in the Fe-Ni-Co-Al-Ta system, i.e. around 10 nm. Several studies revealed and discussed the impact of the size and volume fraction of the β–precipitates on the functional properties in Fe-Mn-Al-Ni SMAs [20,22].

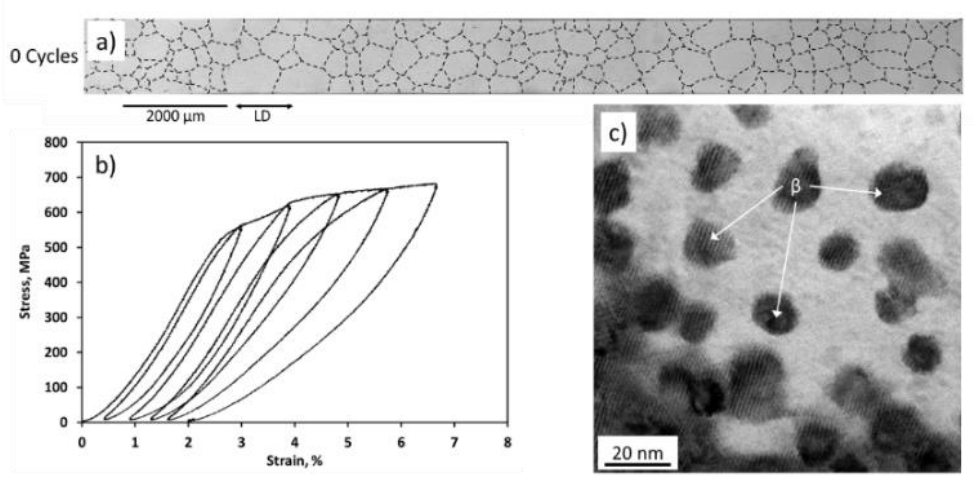

Figure 5: a) Initial microstructure of a polycrystalline Fe-Mn-Al-Ni SMA after solution treatment at 1200 °C for 1h followed by quenching in tempered water; b) pseudoelastic stress-strain curve of a solution treated polycrystalline sample as shown in a) upon aging. c) Finely dispersed β – precipitates upon solutionizing and subsequent aging at 200 °C for 3h.

Figure 5a shows the as cast and solutionized microstructure of a Fe-Mn-Al-Ni SMA tensile sample. Solutionizing and subsequent quenching in tempered water (80 °C) results in evolution of ductile secondary γ–phase at the grain boundaries [23]. Grain sizes range from 500 µm to 1 mm [23]. It is well known that in Fe-Mn-Al-Ni SMAs such microstructures (Figure 5a), i.e. featuring small relative grain size with respect to the cross section [24], result in poor functional properties [24]. This is mainly attributed to intergranular constraints, which are often related to the high anisotropy, i.e. highly pronounced differences in transformation strains in different crystallographic orientations. Consequently, the pseudoelastic behavior of the polycrystalline Fe-Mn-Al-Ni SMA shown in Figure 5b reveals poor shape recovery.

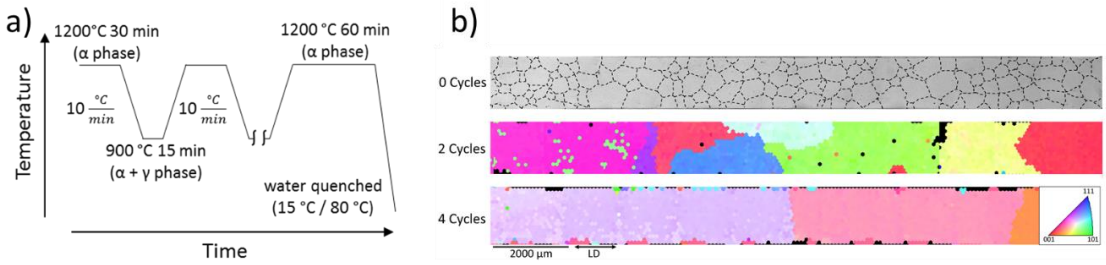

Figure 6: a) Schematic detailing the AGG cyclic heat treatment procedure; b) resulting microstructural appearance upon solutionizing (0 cycles) as well as 2 and 4 cycles of AGG cyclic heat treatment.

In order to promote an increase of the relative grain size and, thus, allow for improved functional properties, Omori et al. [25] introduced a heat treatment method for a Cu-Al-Mn alloy, which leads to abnormal grain growth (AGG) [25]. Expectedly, the functional properties improved remarkably upon AGG [25]. Figure 6a shows a schematic diagram detailing the AGG heat treatment procedure for Fe-Mn-Al-Ni. Upon repeated temperature changes from 1200 °C (α single phase region) to 900 °C (α+γ two phase region) and backwards the microstructure changes as a function of the number of heating-cooling cycles. Figure 6b shows the microstructure evolution after solution treatment (0 cycles), as well as 2 and 4 cycles of AGG treatment. From Figure 6b it is obvious that the grain size increased considerably after cyclic heat treatment. Consequently, a bamboo like microstructure evolved, which shows superior functional properties as was already outlined in several studies [11,23-26].

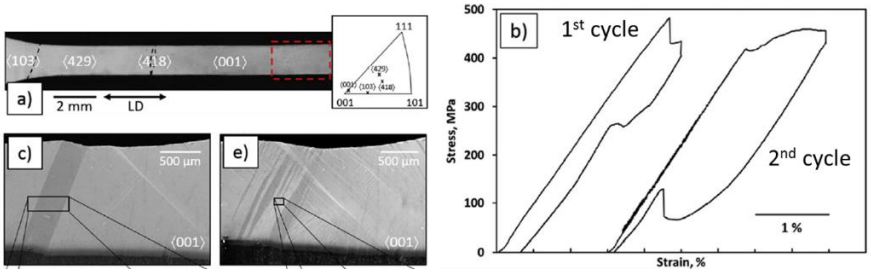

Figure 7: a) Microstructure of the sample subjected to cyclic loading following 4 thermal cycles of the AGG procedure. Crystallographic orientations are indicated on each grain and within the inverse pole figure (inset). The red rectangle in a) represents the AOI shown in c) and d); b) pseudoelastic stress-strain response in the first and second cycle of the sample shown in a). c) and e) show the sample surface during an *in situ* test in the SEM for the first and second cycles, respectively. (Recompiled from [11])

Figure 7a depicts the microstructure of a second sample subjected to cyclic heat treatment. As expected, AGG led to a bamboo like microstructure (Figure 7a). The red rectangle represents the area of interest (AOI) in Figures 7c and 7d. For the first 2 cycles, an *in situ* test was conducted in order to evaluate the martensite variant selection and interaction of variants. In the first cycle mainly one single martensite variant (dark contrast in the SE image, Figure 7c) accommodates the strain, whereas in the second cycle several martensite variants evolve, significantly interacting at the variant-variant boundaries.

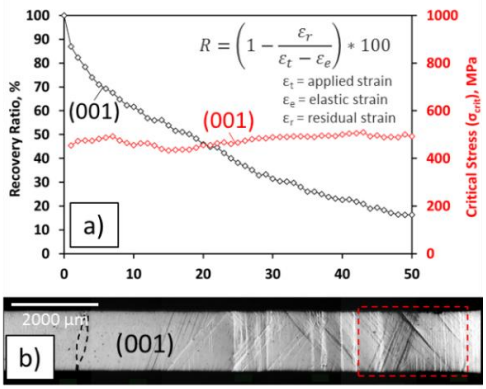

Figure 8: a) Characteristic values extracted from the cyclic stress-strain response: recovery ratio and critical stress evolution vs. cycle number; b) prevailing microstructure after 50 pseudoelastic cycles [11].

Studies in a variety of SMAs focused on the interaction of martensite variants during pseudoelastic transformation and revealed their impact on the functional performance [9,27]. It was shown for Co-Ni-Ga that due to an intensive variant-variant interaction the stress hysteresis drastically increases due to internal friction at the interacting variant boundaries, resulting in an increased dislocation activity [27]. These dislocations are able to mechanically stabilize evolving martensite variants and lead to a distinct cyclic instability, as this was shown for the Fe-Ni-Co-Al-Ta system in the previous chapter [9]. However, it seems that degradation mechanisms in Fe-Mn-Al-Ni and Fe-Ni-Co-Al-Ta SMAs differ significantly. The absolute number of martensite variants and their distribution within the gauge length strongly differ in the first cycle and in the fatigue experiment. One large martensite variant is formed in the first cycle and numerous smaller ones are formed in the second cycle and thereafter (cf. Figs. 7c, 7d and 8b) [11]. The microstructural condition in areas where martensite was already present in a previous cycle seems to change in a way that makes martensitic transformation in the following cycles more difficult. Eventually, this results in the formation of new martensite variants in areas that have not been transformed before (Figs. 7d and 8b).

Figure 8a shows characteristic values extracted from the data obtained by the pseudoelastic fatigue experiments (cf. Fig. 7). Figure 8b depicts the sample surface after 50 pseudoelastic cycles. From Figure 8a it is obvious that the recovery ratio decreased steadily. Finally, only about 15 % of the Fe-Mn-Al-Ni sample shows a reversible phase transformation in cycle 50. The evolution of the critical stress for stress induced phase transformation (σ_{crit}) was analyzed accordingly. It becomes obvious that the degradation mechanisms in Fe-Mn-Al-Ni and Fe-Ni-Co-Al-Ta differ significantly. As can be deduced from Figure 2, σ_{crit} decreases with increasing number of cycles in the Fe-Ni-Co-Al-Ta system. The evolution of σ_{crit} in Figure 8a reveals a constant stress level throughout 50 cycles. This is in good agreement with the discussion on the martensite variant selection related to Figures 7c) and 7d). As in each cycle new martensite variants are activated, the activation energy (needed to form martensite in an area that has not been transformed before) does not change distinctly and, thus, the σ_{crit} level remains constant. Furthermore, the surface relief shown in Figure 8b indicates that upon cyclic loading for 50 cycles a progressive pinning of the evolving martensite variants throughout the transforming grain occurs. In every cycle new variants are formed. Additionally, the interaction of martensite variants may lead to pronounced dislocation activity, similar to the Fe-Ni-Co-Al-Ta [9]. However, evaluation of the impact of the single contributions to the overall degradation seen will be subject of future work.

4 CONCLUSIONS

The current work introduces the nature of degradation in two novel Fe - based SMAs. Analysis of microstructure evolution following pseudoelastic fatigue experiments revealed that degradation mechanism differ significantly comparing both, the Fe-Ni-Co-Al-Ta and Fe-Mn-Al-Ni SMA system. The main findings are as follows:

- Fe-Ni-Co-Al-Ta SMAs show excellent pseudoelastic properties. However, degradation of the functional properties following cyclic loading is seen. Microstructural reasons were found to be related to an increased dislocation activity at the phase and variant boundaries leading to martensite pinning at these sites and the nano-scaled precipitates.
- For the Fe-Mn-Al-Ni SMA system theoretical transformation strains up to 26 % were reported. In single cycle experiments excellent pseudoelastic material behavior is shown, however, in fatigue experiments functional degradation sets in in the very first cycle. Degradation is due to an increased dislocation activity.
- The degradation mechanisms in both SMA systems differ significantly. Whereas pinning of martensite variant boundaries in the Fe-Ni-Co-Al-Ta system occurs mainly in regions, in which martensite variants repeatedly interact, microstructural changes in the Fe-Mn-Al-Ni system can be observed even upon the first phase transformation event. This shifts martensitic transformation to sample volumes that have not been transformed before. Consecutive transformation across the whole sample volume leads to an entirely pinned microstructure upon fatigue.

5 ACKNOWLEDGEMENTS

Funding by Deutsche Forschungsgemeinschaft (DFG) under Contract-No. NI1327/7-1 and SO505/2-2 are gratefully acknowledged. The authors thank I. Karaman, H.J. Maier, W.W. Schmahl, G. Eggeler, A. Weidner, D. Rafaja and H. Biermann for fruitful discussions.

6 REFERENCES

[1] Maki T. In: Otsuka K, Wayman CM, editors. Shape memory materials. Cambridge: Cambridge University Press; 1998;117.
[2] Lagoudas D., (Ed.) Shape Memory Alloys - Modeling and Engineering Applications (Springer, New York, 2008).
[3] Morgan N.B., Mater. Sci. Eng. A, 378 (2004) 16.
[4] Duerig T.W., Melton K.N., Stoeckel D., Wayman C.M.: "Engineering Aspects of Shape Memory Alloys", Butterworth-Heinemann, 1990.
[5] Omori T., Ando K., Okano, M., Xu X., Tanaka Y., Ohnuma I., Kainuma R., Ishida K., Science 68 (2011) 333.
[6] Tanaka Y., Himuro Y., Omori T., Sutou Y., Kainuma R., Ishida K.; Mater. Sci. Eng A, 438 (2006) 1030.
[7] Sehitoglu H., Karaman I., Zhang X.Y., Chumlyakov Y., Maier H.J.; Scripta mater. 44 (20019) 779.
[8] Tanaka Y., Himuro Y., Kainuma R., Sutou Y., Omori T., Ishida K.; Science 327 (2010) 1488.
[9] Krooß P., Somsen C., Niendorf T., Schaper M., Karaman I., Chumlyakov Y., Eggeler G., Maier H.J.; Acta Mater. 79 (2014) 126.
[10] Krooß P., Niendorf T., Karaman I., Chumlyakov Y., Maier H.J.; Funct. Mater. Let. 5 (2012) 4.
[11] Vollmer M. Krooß P., Kriegel M.J., Klemm V., Somsen C., Ozcan H., Karaman I., Weidner A., Rafaja D., Biermann H., Niendorf T.; Scripta Mater. 114 (2016) 156.
[12] Omori, T., Abe S., Tanaka Y., Lee D.Y., Ishida K., Kainuma R.; Scripta Mater. 69 (2013) 812.
[13] Dadda J., Maier H.J., Niklasch D., Karaman I., Karaca H.E., Chumlyakov Y.I., Mater. Trans. A 39 (2008) 2026.
[14] Gall K., Maier H.J.; Acta Mater 50 (2002) 4643.
[15] Gall K., Sehitoglu H., Anderson R., Karaman I., Chumlyakov Y., Kireeva I.; Mater. Sci. Eng., A 317 (2001) 85.
[16] Gall, K., Sehitoglu H., Chumlyakov Y., Kireeva I.; Scripta Mater 40 (1999) 7.
[17] Gall, K., Sehitoglu H., Chumlyakov Y., Kireeva I.; Acta Mater 47 (1999) 1203.
[18] Simon T., Kroeger A., Somsen C., Dlouhy A., Eggeler G.; Acta Mater 58 (2010) 1850.
[19] Tseng LW, Ma J, Karaman I, Wang SJ, Chumlyakov YI. Scripta Mater. 101 (2015) 1.
[20] Tseng L.W., Ma J., Hornbuckle B.C., Karaman I., Thompson G.B., Luo Z.P., Chumlyakov Y.I., Acta Mater. 97 (2015) 234.
[21] Tseng L.W., Ma J., Wang S.J., Karaman I., Kaya M., Luo Z.P., Chumlyakov Y.I., Acta Mater. 89 (2015) 374.
[22] Omori T., Nagasako M., Okano M., Endo K., Kainuma R., Appl. Phys. Let 101 (2012) 1.
[23] Vollmer M., Segel C., Krooß P., Günther J., Tseng L.W., Karaman I., Weidner A., Biermann H., Niendorf T.; Scripta Mater 108 (2015) 23.
[24] Omori T., Okano M., Kainuma R.; APL Mater. 1 (2013) 032103.
[25] Omori T., Kusama T., Kawata S., Ohnuma I., Sutou Y., Araki Y., Ishida K., Kainuma R., Science 341 (2013) 1500.
[26] Omori T., Iwaizako H., Kainuma R.; Mater. Des. 101 (2016) 263.
[27] Dadda J., Maier H.J., Karaman I., Karaca H.E., Chumlyakov Y.I.; Scripta Mater. 55 (2006) 663.